Nature of the transition from two- to three-dimensional ordering in a confined colloidal suspension

Ronen Zangi and Stuart A. Rice
Department of Chemistry and The James Franck Institute, The University of Chicago, Chicago, Illinois 60637
(Received 23 June 1999)

We report the results of extensive molecular dynamics simulations of solid-to-solid transitions in two- to six-layer colloidal suspensions confined between two smooth parallel walls. The studies are designed to elucidate the ordered particle packings that interpolate between the structures of two- and three-dimensional crystals in a confined space. At a fixed density per layer, as the wall separation increases we find a sequence of stable phases, each characterized by uniform amplitude buckling along the normal to the layer planes. The buckling is coupled to an in-plane ordering transition. The buckled phases alternate with phases whose structures contain only parallel planes of particles. The relative densities of the positively and negatively displaced particles in a buckled layer, the in-plane structures, and the behavior with respect to increasing wall separation of the split density distribution that characterizes a buckled layer, clearly identify these layers as intermediates in the reconstructive transformations $n\triangle \rightarrow (n+1)\square$ that occur when the character of the constrained space evolves from being two dimensional to being three dimensional ($\triangle$ denotes layers with hexagonal packing symmetry, while $\square$ denotes layers with square packing symmetry). The two transitions, $n\triangle \rightarrow n$-buckled $\rightarrow (n+1)\square$, are found to be first order.

PACS number(s): 64.70.Dv

I. INTRODUCTION

Since the first observations of ordering in colloidal suspensions, by Perrin in 1909 [1], considerable effort has been devoted to characterizing the evolution of three-dimensional ordering from two-dimensional ordering. In 1983 Pansu, Pieranski and Strzelecki [2] reported the results of experimental studies of a suspension of charged colloidal particles confined in a wedge shaped cell. They showed that as the distance between the confining walls increases the sequence of stable crystal structures is

$$1\triangle \rightarrow 2\square \rightarrow 2\triangle \rightarrow 3\square \rightarrow 3\triangle \rightarrow \cdots . \tag{1.1}$$

In Eq. (1.1), the symbol $\triangle$ denotes crystal slabs with hexagonal (triangular) symmetry, while the symbol $\square$ denotes crystal slabs with square symmetry. This structural route between two- and three-dimensional solids involves two types of reconstructive transformations: first a $(n-1)\triangle \rightarrow n\square$ conversion, and second a $n\square \rightarrow n\triangle$ conversion. A qualitative understanding of the basis for these conversions can be obtained from a study of hard sphere packing between smooth plates. In this case the equilibrium state, in the limit of high pressure, corresponds to maximum volume density [3]. It is found that as the gap between the plates increases, crystal slabs with triangular packing and square packing are alternately most stable. We note that this study does not prove that the structures identified in Eq. (1.1) have the highest density for an arbitrarily chosen slab thickness, since only the structures cited were examined.

Another view of the sequence of transitions displayed in Eq. (1.1) is based on the observation that the one-layer hexagonal and one-layer square symmetries can be related to the (111) and (100) planes in a face centered cubic (fcc) crystal, respectively. Then the sequence in Eq. (1.1) can be viewed as the result of slicing n layers with different orientations of the fcc structure. As noted in Ref. [3], there are several reasons for not accepting this interpretation, and it is one of the goals of our work to show that the transitions depicted in Eq. (1.1) are not aptly described as associated with slices of a three-dimensional fcc crystal.

The structural sequence displayed in Eq. (1.1), which includes only hexagonal and square symmetries, implies that increasing the wall separation leads only to integral numbers of layers in the available space. When the number of layers is small there will then be large fluctuations in density and pressure. Hence, when the available gap is greater than that needed for the $n\triangle$ structure but smaller than that needed for the $(n+1)\square$ structure, instability with respect to other structures can occur. Consider, for example, a one-layer system. In this system the in-plane packing structure is hexagonal, and the density distribution along the normal to the plane (which we call the longitudinal density distribution) can have one peak, corresponding to one layer with thermal motion normal to the layer, or it can have two peaks, corresponding to one layer adjacent to each wall. Each of these layers also supports thermal motion normal to the plane. The buckling of a plane of particles is coupled to an in-plane order-disorder transition. Specifically, the lateral positions of particles that are localized at the same height are ordered. This ordering can take the form of linear or zigzag single rows of particles, and a well ordered phase appears when there are nonoverlapping split peaks in the longitudinal density distribution. Such transitions have been observed in single-layer colloidal suspensions in experiments [4–7] and in computer simulation studies [9,14]. These results also follow from an analysis based on the Landau theory of phase transitions, in which the thermodynamic potential is expanded about that for the flat state [8], and from an analysis based on free-volume theory [9]. It is found that the stability region of the buckled phase increases with the gap between the confining walls until the buckled phase becomes unstable with respect

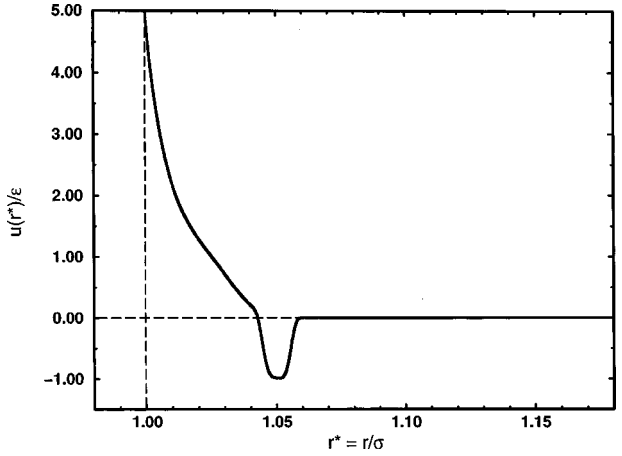

FIG. 1. Marcus-Rice-type potential.

to the formation of a crystal with an additional layer. The formation of a buckled phase reduces the density fluctuations when the distance between the confining walls is increased. An examination of the symmetry of the emerging up and down phases for a single layer leads to the suggestion that the buckled phase is an intermediate structure between one-layer hexagonal and two-layer square lattices [9]. It is worth noting that the buckling transition is not restricted to colloidal systems; it has also been observed in amphiphilic membranes [10–12] and in Langmuir monolayers [13]. The experimental observations are backed up by the results of computer simulation studies of confined hard spheres [9], of confined particles with soft repulsive interactions [14], and

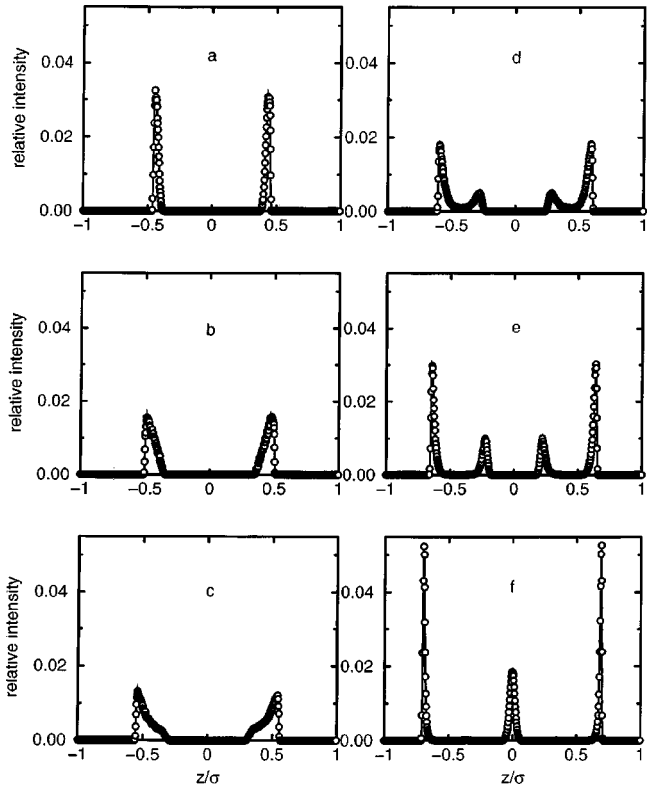

FIG. 2. Longitudinal density distributions at constant lateral pressure ($p_l^*=45$) and temperature. (a) $H=1.90\sigma$, (b) $H=2.00\sigma$, (c) $H=2.10\sigma$, (d) $H=2.20\sigma$, (e) $H=2.30\sigma$, and (f) $H=2.40\sigma$.

TABLE I. The values of $\mathcal{D}$ [in Eq. (2.2)] and the wall separation H.

$\mathcal{D}$	H/σ
1×10^{51}	1.80
5×10^{43}	1.90
2×10^{38}	2.00
1×10^{33}	2.10
1×10^{28}	2.20
1×10^{24}	2.30
1×10^{22}	2.35
1×10^{20}	2.40
1×10^{6}	2.82
1×10^{3}	2.90
1×10^{0}	3.02
1×10^{-5}	3.20
5×10^{-7}	3.25
1×10^{-8}	3.30
1×10^{-17}	3.74
1×10^{-20}	3.90
1×10^{-23}	4.05
1×10^{-26}	4.20
1×10^{-32}	4.59
5×10^{-46}	5.58

of confined particles with soft repulsive and attractive interactions [14]. The results obtained from the studies of the hard sphere system suggest that the buckling transition may be entropy induced. This inference follows from the observation that, in an inhomogenuous system, the in-plane direction is distinct from the out-of-plane direction, and there is a competition between the in-plane and out-of-plane motions of the particles.

In this paper we report the results of extensive molecular dynamics simulations of the buckling transition in multilayer systems enclosed between parallel smooth planar walls. We find that, as for the case of the one-layer buckling transition, the multilayer buckling transitions are characterized by a

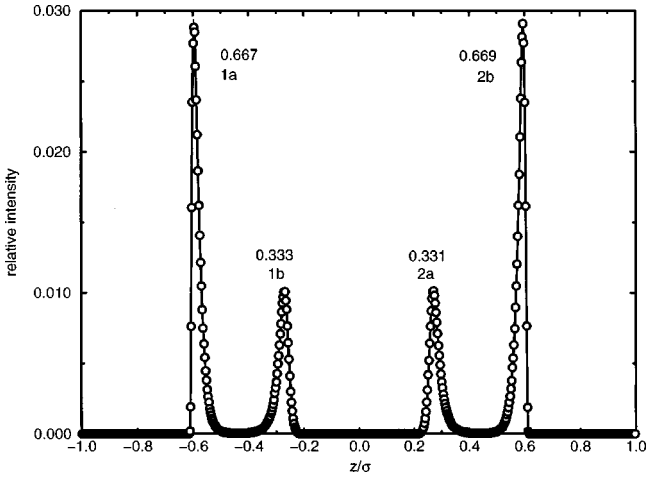

FIG. 3. Two-layer buckling. The longitudinal density profile for $H=2.20\sigma$ and $\rho_{2D}^*=1.1000$ (volume fraction=0.523). The fraction near each peak is the number of particles that corresponds to this peak divided by N_{layer}.

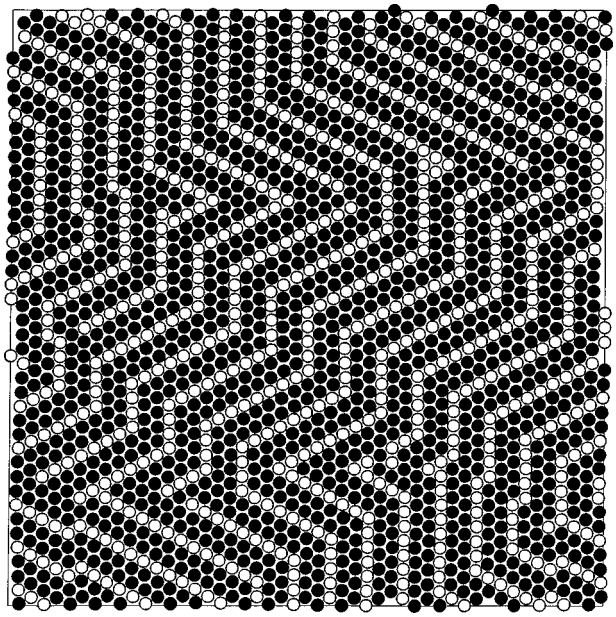

FIG. 4. Two-layer buckling: two rows are buckled against a single row. The lateral configuration of the upper layer in Fig. 3. The particles that correspond to peak $2a$ are denoted by empty circles, and those that correspond to peak $2b$ by black circles.

two-peaked longitudinal density distribution for each layer, and are coupled to an in-plane ordering transition. The relative densities, the in-plane structure, and the behavior upon increasing the wall separation of the longitudinal density distribution clearly imply that these buckled phases interpolate the reconstructive transformations $n\triangle \rightarrow (n+1)\square$. The two transitions, $n\triangle \rightarrow n$-buckled$\rightarrow (n+1)\square$, are found to be first order.

The other type of transition that occurs when crystalline structures evolve between two and three dimensions, $n\square \rightarrow n\triangle$, is the subject of current research and will be described in a later publication. The preliminary results obtained from simulations of a two-layer system suggest that this conversion is potential dependent and can involve a rhombic phase as an intermediate.

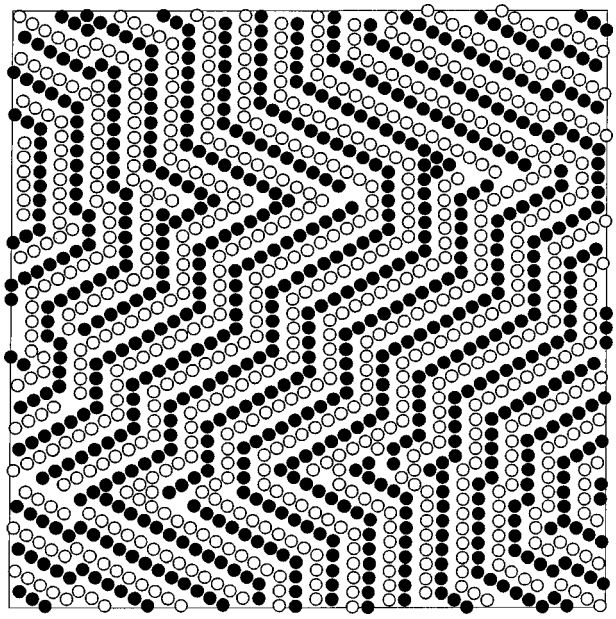

FIG. 5. Two-layer buckling. The lateral correlation of the two inner peaks in Fig. 3. The particles that correspond to peak $2a$ are denoted by black circles, and those that correspond to peak $1b$ by empty circles.

TABLE II. The phase boundary of the two-layer ordered buckled phase for different values of the wall separation (the numbers shown are the lowest values of ρ_{2D}^{*} that support this phase).

H/σ	ρ_{2D}^{*}
2.00	1.150
2.10	1.120
2.20	1.100
2.30	1.090

II. MODEL SYSTEM AND COMPUTATIONAL DETAILS

The model systems that we have studied consist of 2–6 layers of particles, each layer containing 2016 particles. The particles are contained in a simulation box which is rectangular in the xy plane, with side lengths in the ratio $x:y = 7:(8\sqrt{3}/2)$. Periodic boundary conditions were imposed in the x and y directions, but not in the z direction. To confine the particles to a slab of specified thickness, H, they were subjected to a one-body external potential in the z direction (see below).

We find it convenient to use the reduced variables $r^{*} = r/\sigma$, $z^{*} = z/\sigma$, $T^{*} = k_B T/\varepsilon$, $\rho^{*} = \rho\sigma^2$, and $m = 1$, with σ the diameter of the particle, ε the depth of the attractive potential well, ρ the number density, and m the mass of the particle. The systems we have studied all have high density.

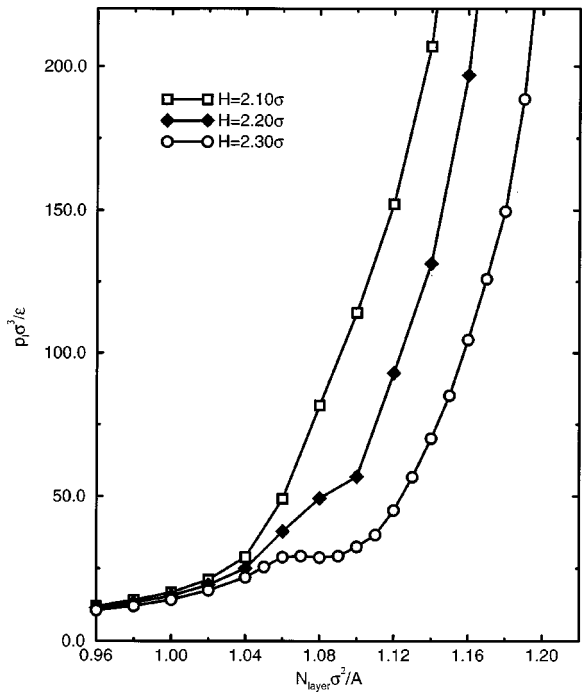

FIG. 6. The lateral pressure as a function of the one-layer two-dimensional number density, indicating the $2\triangle \rightarrow$two-layer-buckled transition when $2.10\sigma \leqslant H \leqslant 2.30\sigma$.

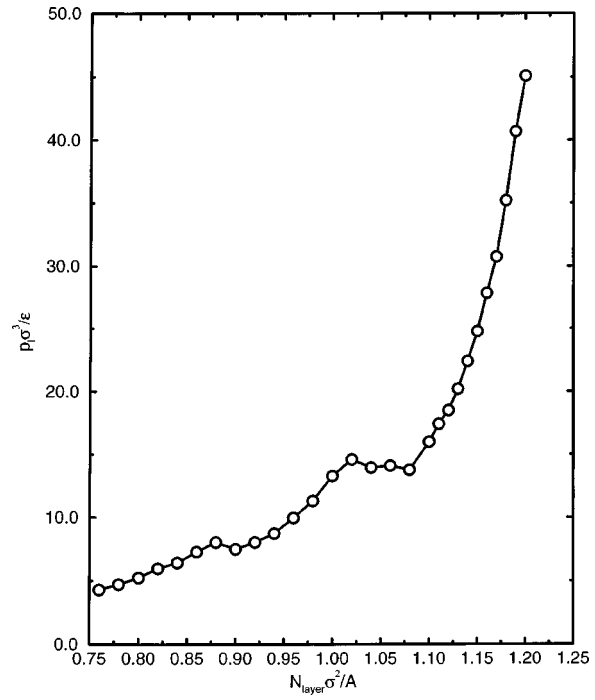

FIG. 7. The lateral pressure as a function of the one-layer two-dimensional number density, indicating the two-layer-buckled→3□ transition when $H=2.40\sigma$.

Consequently, although the particles can move in the z direction, from one layer to another, on average the number of particles in each layer is the same. Therefore, we choose to characterize the state of the system with the one-layer two-dimensional (2D) number density $\rho_{2D}=N_{\text{layer}}/A$, where A is the area of the simulation cell in the xy plane, and N_{layer} is the average number of particles per layer.

The majority of our calculations were carried out for particles subject to the same pair interaction as used in our previous work, namely,

$$u(r^*)=-\varepsilon\exp\left[-\left(\frac{r^*-wc^*}{ww^*}\right)^4\right]+2\times10^{-19}\left(r^*-\frac{1}{2}\right)^{-64}+1.2\exp\left[-\left(\frac{r^*-0.96}{0.074}\right)^8\right]. \tag{2.1}$$

This pair potential (see Fig. 1) was designed by Marcus and Rice to have the features of colloidal particles that are sterically stabilized by grafted polymer brushes to prevent aggregation induced by van der Waals forces. The first term in Eq. (2.1) represents the attraction between colloid particles when there is incipient overlap between the stabilizing brushes on their surfaces; for simplicity we have taken the functional form of this attraction to be an inverse even power exponent with depth $\varepsilon=1.0k_BT$ and width $ww/\sigma=ww^*=0.006$, centered at $wc^*=1.05$. The second term in Eq. (2.1) is the core-core repulsion, which is the dominant contribution to $u(r^*)$ when $r^*\leqslant 1$; the functional form chosen is very nearly a hard core repulsion but has continuous derivatives. The last term in Eq. (2.1) is an interpolating soft repulsion, representing the entropy cost associated with interpenetration of the stabilizing brushes attached to the surfaces of the colloid particles; it plays the role of a spline function between the aforementioned attractive and repulsive terms.

The confinement of the particles in the $\pm z$ directions is affected by the action of a one body z dependent external field. Different forms can be chosen for this field, the simplest being that for hard parallel walls. Then the extra degree of freedom that is introduced in the thermodynamic description of the system is the spacing between those two walls. Because of their macroscopic size, colloidal spheres do not ''feel'' the atomic scale granularity of the walls, so the walls can be regarded as smooth. The shape of the potential we have chosen,

$$u_{\text{ext}}(z^*)=\mathcal{D}\varepsilon(z^*)^{\zeta}, \tag{2.2}$$

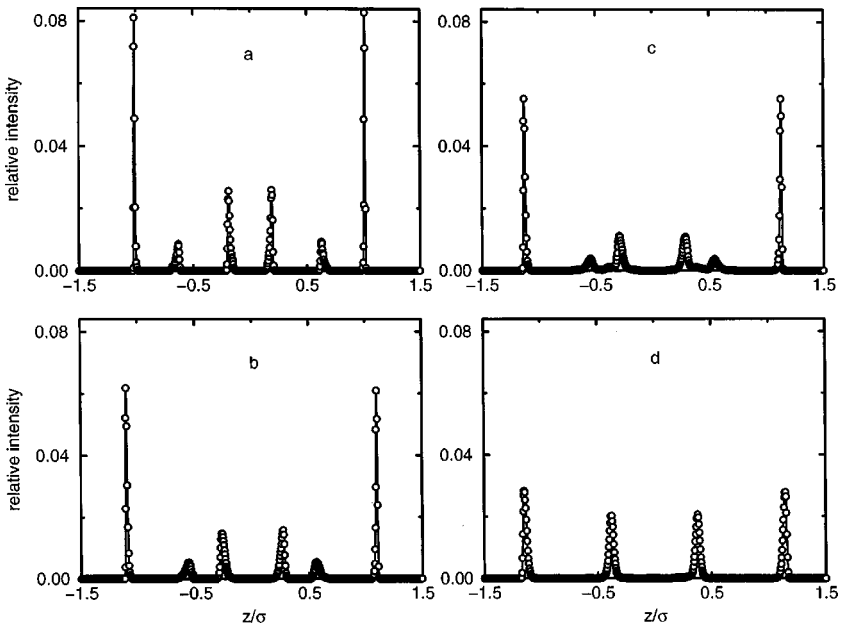

FIG. 8. The longitudinal density distributions at constant N, A, and T ($\rho_{2D}^*=1.2000$), for the three-layer-buckled→4□ transition. (a) $H=3.02\sigma$, (b) $H=3.20\sigma$, (c) $H=3.25\sigma$, and (d) $H=3.30\sigma$.

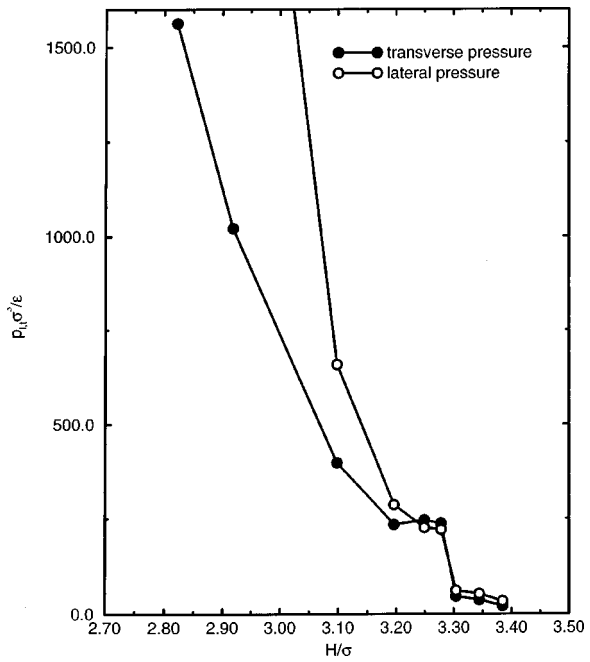

FIG. 9. The lateral (empty circles) and transverse (filled circles) pressures as a function of the height between the two confining walls at constant N, A, and T ($\rho^*_{2D}=1.2000$), indicating the three-layer-buckled→4□ transition.

is such as to confine the system to form a slab with well specified height H. In Eq. (2.2), z^* is the distance from the center of the cell to the center of mass of the particle and $\zeta=128$. The value of $\mathcal{D}$ determines the distance H between the walls. Table I displays the values of $\mathcal{D}$ and the corresponding values of H.

The lateral and transverse pressures p_l and p_t, respectively, were calculated from the lateral and transverse virials $\mathcal{W}_l$ and $\mathcal{W}_t$, where

$$\mathcal{W}_l=-\frac{1}{2}\sum_{i=1}^{N}\sum_{j>i}^{N}\frac{x_{ij}^2+y_{ij}^2}{r_{ij}}\frac{\partial u(r)}{\partial r}\bigg|_{r=r_{ij}}, \tag{2.3a}$$

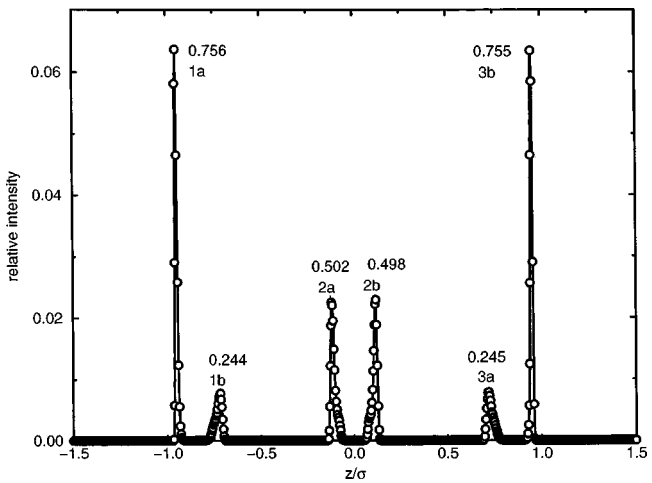

FIG. 10. Three-layer buckling. The longitudinal density profile for $H=2.90\sigma$ and $\rho^*_{2D}=1.1600$ (the volume fraction is 0.628). The fraction near each peak is the number of particles that corresponds to this peak divided by N_{layer}.

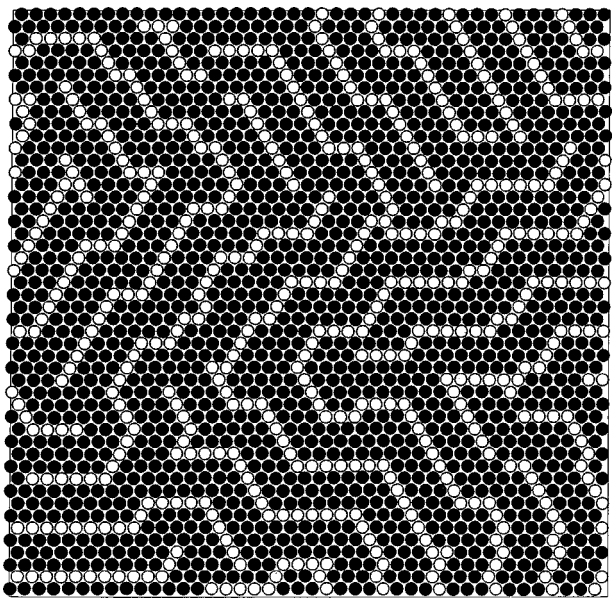

FIG. 11. Three-layer buckling: three rows are buckled against a single row. The lateral configuration of the upper layer in Fig. 10. The particles that correspond to peak $3a$ are denoted by empty circles, and those that correspond to peak $3b$ by black circles.

$$\mathcal{W}_t=-\frac{1}{2}\sum_{i=1}^{N}\sum_{j>i}^{N}\frac{z_{ij}^2}{r_{ij}}\frac{\partial u(r)}{\partial r}\bigg|_{r=r_{ij}}. \tag{2.3b}$$

We find

$$p_l=\frac{Nk_BT+\langle\mathcal{W}_l\rangle}{V}, \tag{2.4a}$$

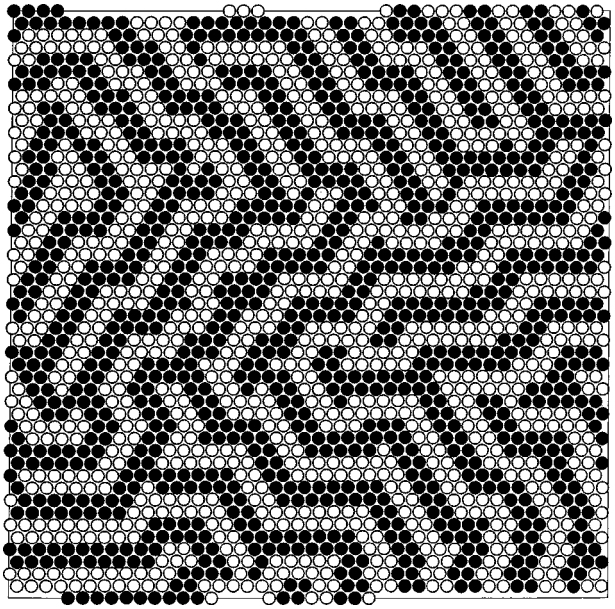

FIG. 12. Three-layer buckling: two rows are buckled against two rows. The lateral configuration of the middle layer in Fig. 10. The particles that correspond to peak $2a$ are denoted by empty circles, and those that correspond to peak $2b$ by black circles.

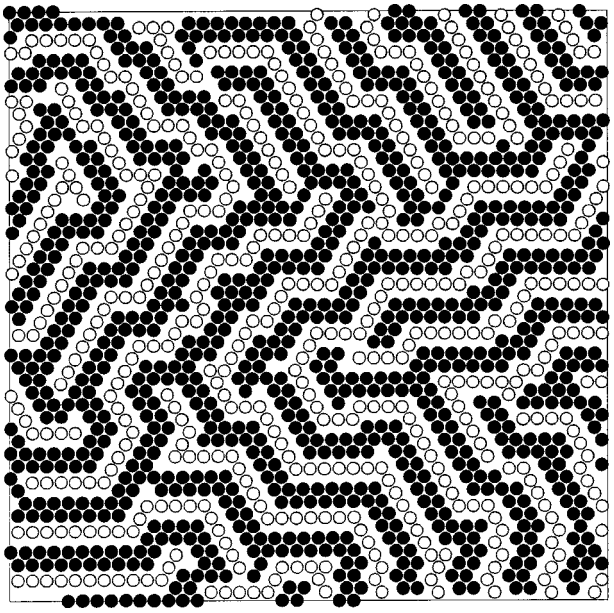

FIG. 13. Three-layer buckling. The lateral correlation of the outer layer inner peak and the middle layer peak in Fig. 10. The particles that correspond to peak $3a$ are denoted by empty circles, and those that correspond to peak $2b$ by black circles.

$$p_t = \frac{Nk_BT + 2\langle \mathcal{W}_t \rangle}{V'}, \tag{2.4b}$$

where $V' = Ah$ and $H = \sigma + h$.

The molecular dynamics (MD) simulations were carried out using the velocity Verlet algorithm and the Verlet neighbor list method for the calculation of the potential energy. The distance at which the potential was cut off was 1.5σ, and the neighbor list cut off was 2.4 times the projected in-plane average spacing of the particles. The need for updating of the neighbor list was checked at every time step. The average time step used was, in reduced units, 5×10^{-4}; the associated rms fluctuation in total energy did not exceed one part in 10^5. Each density was equilibrated for at least 1×10^7 MD steps, and then data collected for 4×10^4 MD steps, every 400 time steps.

The initial configuration for each of the simulations was taken to be a perfect triangular lattice, with the positions of the layers symmetric with respect to the midpoint of the cell ($z^*=0$). In the initial configuration all the particles of each layer were assigned the same value of z^*. The lattice points of the layers were arranged out of registry with respect to one another. For a number of layers equal to or greater than three we took the *ABA* type structure of the hexagonal close

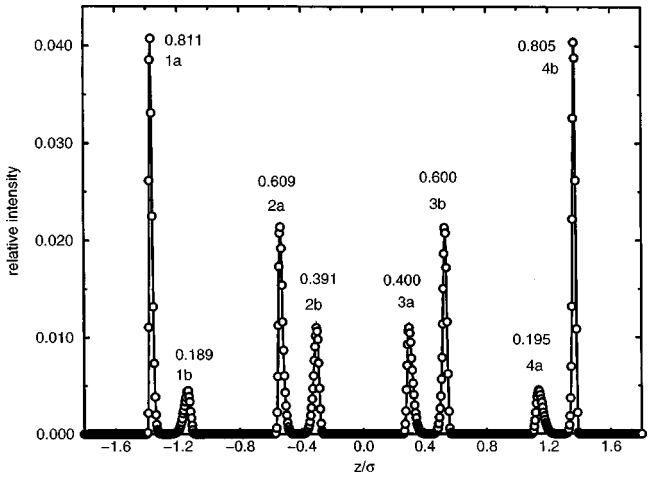

FIG. 14. Four-layer buckling. The longitudinal density profile for $H=3.74\sigma$ and $\rho^*_{2D}=1.1600$ (the volume fraction is 0.650). The fraction near each peak is the number of particles that corresponds to this peak divided by N_{layer}.

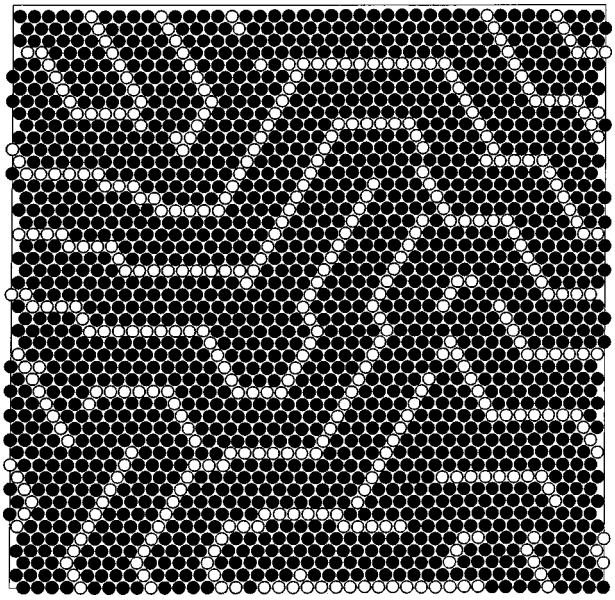

FIG. 15. Four-layer buckling: four rows are buckled against a single row. The lateral configuration of the upper outer layer in Fig. 14. The particles that correspond to peak $4a$ are denoted by empty circles, and those that correspond to peak $4b$ by black circles.

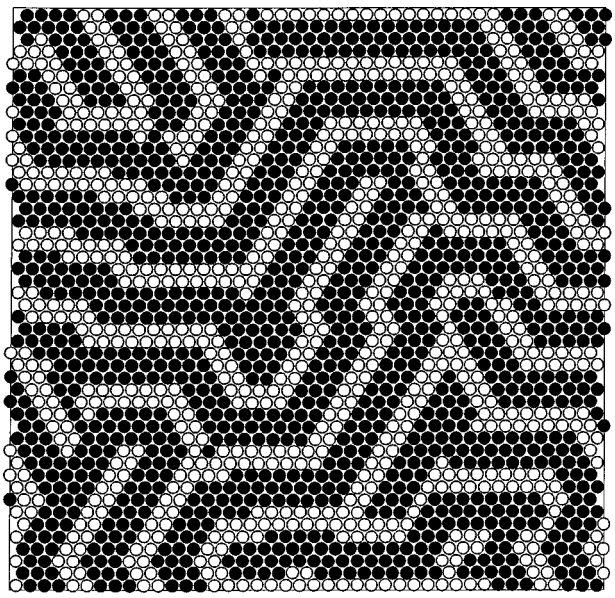

FIG. 16. Four-layer buckling: three rows are buckled against two rows. The lateral configuration of the upper inner layer in Fig. 14. The particles that correspond to peak $3a$ are denoted by empty circles, and those that correspond to peak $3b$ by black circles.

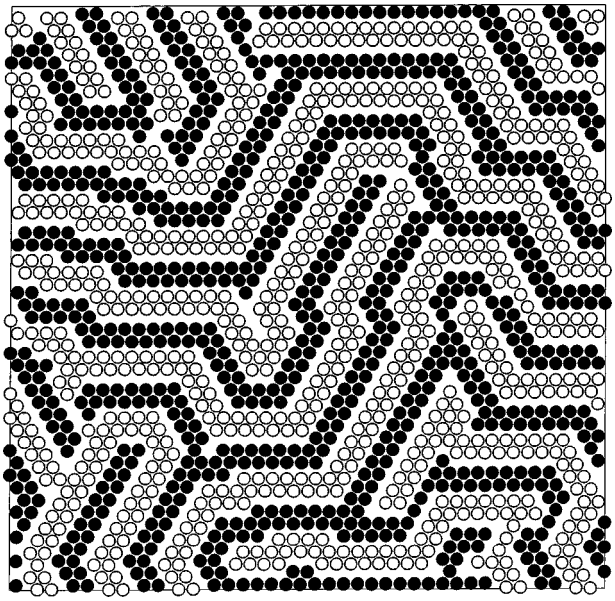

FIG. 17. Four-layer buckling. The lateral correlation between peaks $2b$ (empty circles) and $3a$ (black circles) of Fig. 14.

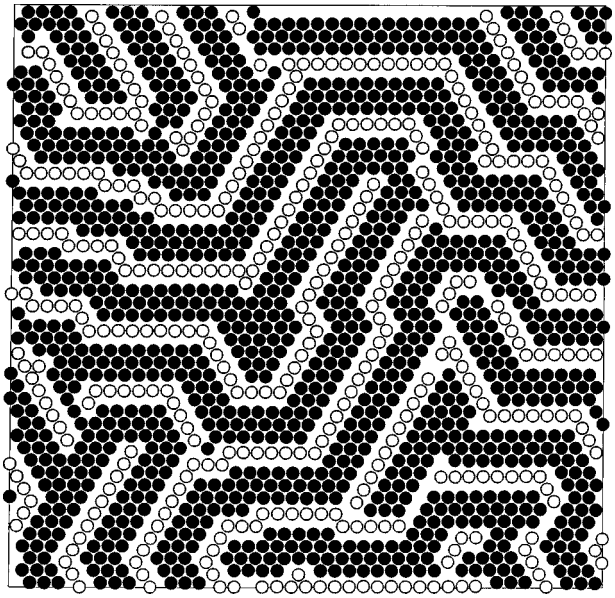

FIG. 18. Four-layer buckling. The lateral correlation between peaks $4a$ (empty circles) and $3b$ (black circles) of Fig. 14.

packed lattice. All of the simulations results reported in this paper refer to the reduced temperature $T^*=1.00$.

III. RESULTS

A. Two-layer buckling transition

We have studied the behavior of two-layer colloidal suspensions confined between walls with gaps in the range $1.80\sigma \leqslant H \leqslant 2.40\sigma$. The behavior of the longitudinal density distribution as a function of wall separation is shown in Fig. 2. The several cases shown describe a path that corresponds to equilibrium between a confined slab and bulk, i.e., a path along which there is equality of temperature and lateral pressure between the two phases. When $H=1.90\sigma$ the longitudinal density distributions of the layers adjacent to each wall are unimodal. As H increases the longitudinal density distribution of each layer becomes bimodal, and the peaks at smaller $|z^*|$ move continuously toward $z^*=0$. When $H=2.40\sigma$ these peaks merge and the system consists of three ordered layers with square packing in each layer. An analysis of the amplitudes of the peaks in the longitudinal density distributions (Fig. 3) shows that each layer is split into a and b components in such a way that two-third of the particles are displaced towards the walls $(1a,2b)$, while one-third of the particles are shifted toward the center $(1b,2a)$. An examination of the in-plane structure of one of the layers (Fig. 4) reveals that the a and b layers are associated with an ordered phase in which two rows are displaced toward the wall with respect to one row.

How does the structure of the two-layer buckled phase mediate the $2\triangle \rightarrow 3\square$ conversion? The transformation of the layers corresponding to the outer peaks ($1a$ and $2b$) to square layers is similar to the way the one layer buckled phase mediates the $1\triangle$ to $2\square$ transition. An examination of the particle configuration displayed in Fig. 4 shows that decreasing the distance between the paired rows (corresponding to peak $1a$ or peak $2b$) along the perpendicular between them creates a layer which has half square packing and half triangular packing. Similarly, an examination of the particle configuration displayed in Fig. 5, which represents the superposed lateral configurations in layers $1b$ and $2a$, shows that decreasing the distance between the rows along the perpendicular between them creates the same situation where half of the layer has square packing and half has triangular packing. With rearrangement of the triangular packing present in each layer to square packing the overall effect is then to form the $3\square$ structure.

The stability region of the buckled phase increases with increasing H, and ordered buckled phases were observed for $2.00\sigma \leqslant H \leqslant 2.35\sigma$. When $1.80\sigma \leqslant H \leqslant 1.90\sigma$ the buckled phase is not stable and the longitudinal density distribution is unimodal for each of the layers. The buckled phase corresponds to the high density region in the phase diagram. The lowest density at each value of H for which the two layer ordered buckled phase is stable is given in Table II. When $H=2.40\sigma$ the ordered two-layer buckled phase is unstable with respect to a three-layer slab with body centered cubic (bcc) structure.

An examination of the distribution of interparticle distances for the model system with Marcus-Rice-type interactions, for different wall separations and densities that support two-layer buckling, reveals that both the intralayer and interlayer particle separations can (i) be all on the soft repulsive part of the potential curve, (ii) be all at the minimum of the attractive well, or (iii) exhibit coexistence of separations of types (i) and (ii).

The buckling transition appears to be universal in the sense that it does not depend on the type of interparticle potential used. Most of our simulations were executed with the Marcus-Rice potential, but a few simulations were carried out using a modified Marcus-Rice potential with the attractive well removed; this potential has only soft and hard core repulsions. A similar small set of simulations was carried out using the hard sphere potential. All of these potentials support ordered buckling of the layers in the simulation sample.

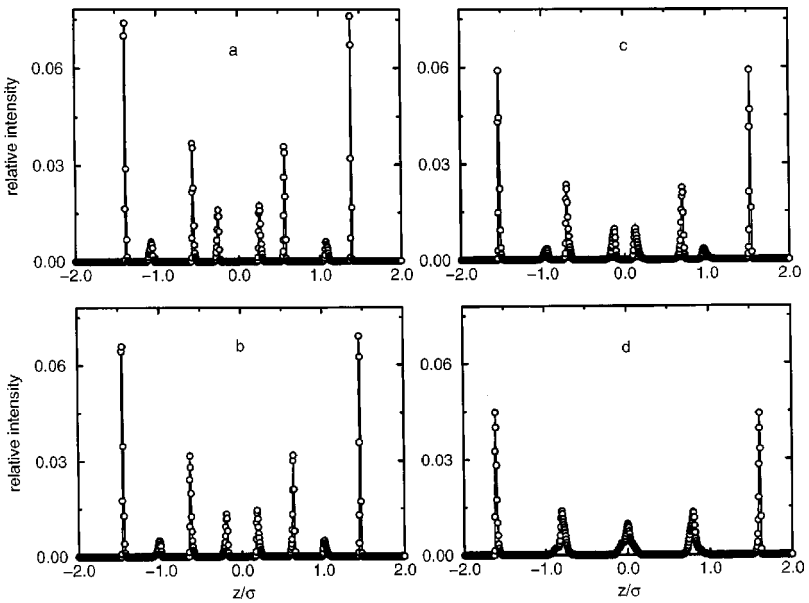

FIG. 19. The longitudinal density distributions at constant N, A, and T ($\rho^*_{2D}=1.2000$), for the four-layer-buckled→5□ transition. (a) $H=3.75\sigma$, (b) $H=3.90\sigma$, (c) $H=4.05\sigma$, and (d) $H=4.20\sigma$.

Figure 6 displays the isotherms of the lateral pressure as a function of the one-layer two-dimensional number density. For $H=2.30\sigma$ a van der Waals loop is evident in the range $1.0500\leqslant\rho^*_{2D}\leqslant1.0900$. The width of the van der Waals loop decreases as H decreases, and for $H\leqslant2.10\sigma$ the lateral pressure isotherm appears to be continuous on the scale of the sampling of the density that we have used in our calculations. However, the difference between the densities of the coexisting buckled and unbuckled phases decreases with decreasing H, and we cannot rule out the possibility that when H is small this difference is smaller than the sampling interval for the density. If so, what appears to be a continuous transition when $H\leqslant2.10\sigma$ remains a weak first order transition. Just this behavior was encountered in our study of the buckling of a single layer when $H=1.20\sigma$, which value of H is close to the critical value below which the buckled phase is unstable at all densities.

The two-layer buckled phase to 3□ transition is also first order, as can be seen from the lateral pressure isotherm for $H=2.40\sigma$ (Fig. 7); this isotherm clearly displays a van der Waals loop for $1.0000\leqslant\rho^*_{2D}\leqslant1.0800$. Examination of the lateral configurations for systems with densities inside the coexistence region confirms the separation of the two phases. When $\rho^*_{2D}\leqslant1.0000$ the system is in a two-layer-buckled phase, but the displaced particles are not laterally ordered. For densities $\rho^*_{2D}\geqslant1.0800$ the system has a 3□ structure. Note that the smaller van der Waals loop in the density range $0.8600\leqslant\rho^*_{2D}\leqslant0.9200$ corresponds to the melting transition. The solid close to the melting point is in a triangular lattice. The longitudinal density distribution of each of the layers of this lattice has one peak, with a shoulder corresponding to a strong overlap with the displaced peaks of the longitudinal density distribution of the buckled phase.

B. Three-layer buckling transitions

We have studied the behavior of three-layer colloidal suspensions confined between walls with gaps in the range $2.82\sigma\leqslant H\leqslant3.39\sigma$. The transformation of a three-layer buckled phase system to a four-layer system with bcc structure, along a path at constant A, N, and T, is shown in Fig. 8. The confinement range covered is $3.02\sigma\leqslant H\leqslant3.30\sigma$. As before, the longitudinal density distribution for each of the three layers is bimodal. Note that as H increases the inner peaks (smaller $|z^*|$) of the longitudinal density distributions of the layers adjacent to the walls move to smaller values of $|z^*|$, while the outer peaks of those distributions move toward larger values of $|z^*|$. Simultaneously, the longitudinal density distribution of the inner layer of the three-layer system splits into two distributions with equal amplitude, and each of these moves toward larger values of $|z^*|$ as H increases. Eventually, when $H\geqslant3.30\sigma$, the peaks merge to form a 4□ structure. When $H=3.25\sigma$ the results of our simulations show coexistence between a three-layer buckled phase and a 4□ phase. The longitudinal density distribution at this value of H shows that, in addition to the peaks of the buckled layers, two additional peaks start to build up around $|z^*|=0.4$, a location where at higher values of H (e.g., $H=3.30\sigma$) we found the two newly formed layers of 4□ structure. The lateral and transverse pressures as a function of H are shown in Fig. 9. Both isotherms have a van der Waals

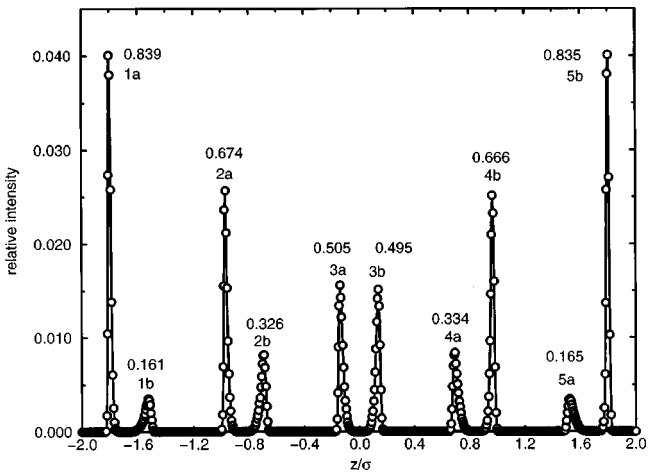

FIG. 20. Five-layer buckling. The longitudinal density distributions for $H=4.59\sigma$ and $\rho^*_{2D}=1.1600$ (the volume fraction is 0.662). The fraction near each peak is the number of particles that corresponds to this peak divided by N_{layer}.

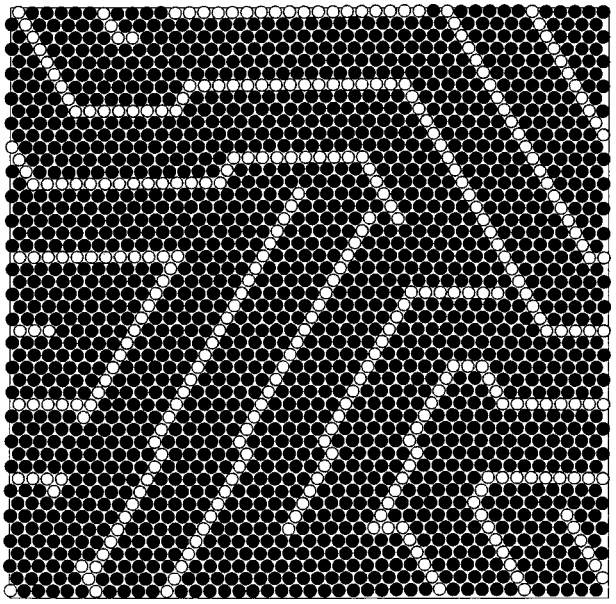

FIG. 21. Five-layer buckling: five rows are buckled against a single row. The lateral configuration of layer 5 in Fig. 20. The particles that correspond to peak $5a$ are denoted by empty circles, and those that correspond to peak $5b$ by black circles.

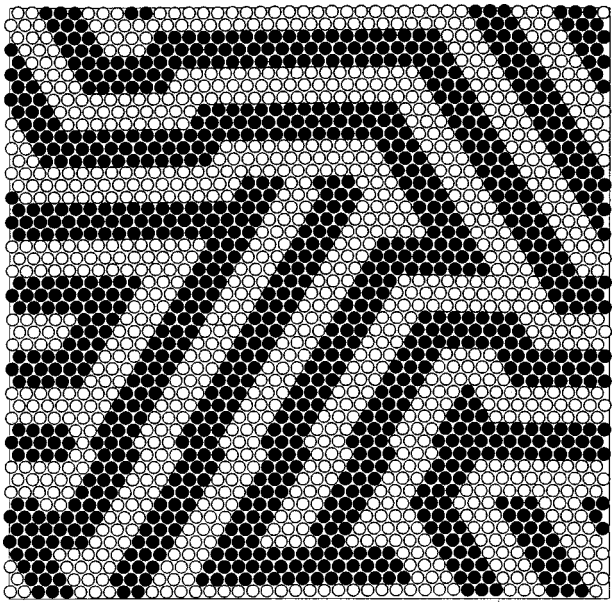

FIG. 23. Five-layer buckling: three rows are buckled against three rows. The lateral configuration of layer 3 in Fig. 20. The particles that correspond to peak $3a$ are denoted by empty circles, and those that correspond to peak $3b$ by black circles.

loop, confirming that the transition occurs in both the lateral and normal directions and that the transition is first order.

Figure 10 displays the amplitudes of the peaks in the longitudinal density distributions of the layers. The amplitude ratio of the outer layer distributions show that three-fourths of the particles ($1a$,$3b$) are displaced toward the walls, and one-fourth of the particles ($1b$,$3a$) are displaced toward smaller $|z^*|$. The longitudinal density distribution of the central layer ($2a$,$2b$) splits into two equal amplitude distributions. The numbers of particles in the layers associated with each of the peaks in the longitudinal density distributions is such that the combination of adjacent buckled layers to form four unbuckled layers yields a $4\square$ structure. This can be seen from the particle configuration in an outer layer (Fig. 11) and in an inner layer (Fig. 12). The former clearly shows the coherent displacement of three rows of particles with respect to a single row, and the latter clearly shows two rows of particles that are displaced toward larger $|z^*|$ and two rows that are displaced toward smaller $|z^*|$. Examination of the lateral correlation between the particles corresponding to peaks $2b$ and $3a$ in Fig. 13, and the outer layer configuration $3b$, reveals that two-third of the arrangement has a hexagonal configuration and one-third has a square configuration. Then, the same type of rearrangements can be exploited in

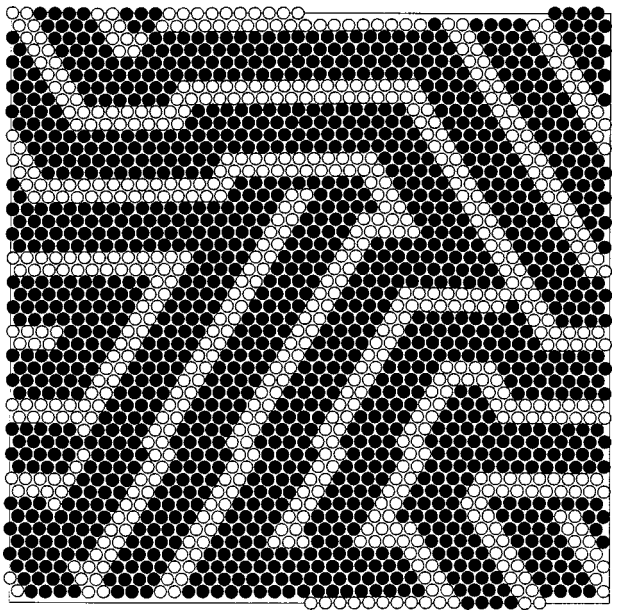

FIG. 22. Five-layer buckling: four rows are buckled against two rows. The lateral configuration of layer 4 in Fig. 20. The particles that correspond to peak $4a$ are denoted by empty circles, and those that correspond to peak $4b$ by black circles.

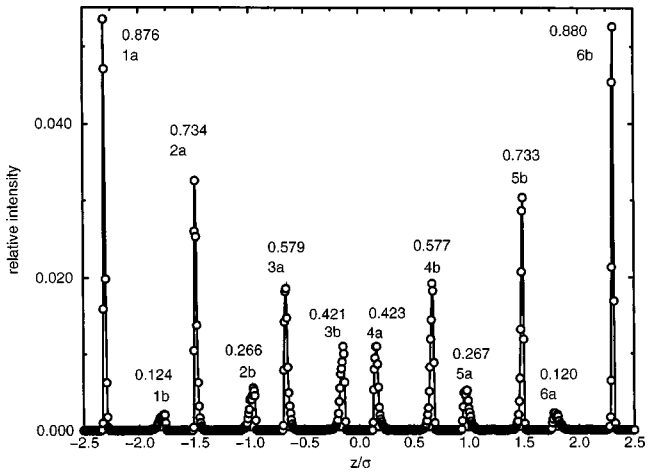

FIG. 24. Six-layer buckling. The longitudinal density distribution for $H=5.58\sigma$ and $\rho^*_{2D}=1.2000$ (the volume fraction is 0.676). The fraction near each peak is the number of particles that corresponds to this peak divided by N_{layer}.

all four layers to convert the three-layer buckled phase to a phase with 4□ packing.

C. Four-layer buckling transitions

The amplitudes of the peaks in the longitudinal density distributions for the buckled phase of four layers ($H=3.74\sigma$ and $\rho_{2D}^{*}=1.1600$) are shown in Fig. 14. The buckling transition in this system shows the same trend as that in systems with smaller numbers of layers. Specifically, the distribution of particles in the outer layers splits such that four-fifths of the particles move toward the walls and one-fourth of the particles moves toward smaller $|z^{*}|$, while the numbers of particles in the two middle layers each split in the ratios $\frac{3}{5}$ and $\frac{2}{5}$. Then, by combining pairs of density distributions, specifically, $1b$ and $2a$, $2b$ and $3a$, and $3b$ and $4a$, we obtain five layers with the same number of particles. The lateral structure of the upper outer layer (Fig. 15) shows that four rows of particles are buckled against a single row, and the lateral structure of the upper middle layer (Fig. 16) shows that three rows of particles are buckled with respect to two rows. The lateral correlations between the particles, corresponding to peaks $2b$ and $3a$, and $3b$ and $4a$, are shown in Figs. 17 and 18, respectively.

The behavior of the longitudinal density distribution of the buckled phase along a path at constant A, N, and T, for four different values of H in the range $3.75\sigma \leqslant H \leqslant 4.20\sigma$, is shown in Fig. 19. For $H=4.20\sigma$ we find that there is coexistence between a four-layer buckled phase and a 5□ phase.

D. Five- and six-layer buckling transitions

The amplitudes of the peaks in the longitudinal density distributions for the buckled phase of five layers ($H=4.59\sigma$ and $\rho_{2D}^{*}=1.1600$) are shown in Fig. 20. The particles in the layers that are labeled 1 and 5 split in ratios of $\frac{5}{6}$ $(1a,5b)$ and $\frac{1}{6}$ $(1b,5a)$, those that are labeled 2 and 4 split in ratios of $\frac{4}{6}$ $(2a,4b)$ and $\frac{2}{6}$ $(2b,4a)$, and those in the middle layer (labeled 3) split in ratios of $\frac{3}{6}$ and $\frac{3}{6}$. The lateral structure of layer 5 $(5a,5b)$ is shown in Fig. 21, that of layer 4 $(4a,4b)$ is shown in Fig. 22, and that of layer 3 $(3a,3b)$ is shown in Fig. 23. The correlations of the particles that correspond to the split peaks to be merged show behavior similar to that observed for the smaller numbers of layers.

The longitudinal density profile for six layer buckling is shown in Fig. 24 for $H=5.58$ and $\rho_{2D}^{*}=1.2000$. The layers that are close to the walls, 1 and 6, split in ratios of $\frac{6}{7}$ and$\frac{1}{7}$. Layers 2 and 5 split in ratios of $\frac{5}{7}$ and $\frac{2}{7}$, and layers 3 and 4 split in ratios of $\frac{4}{7}$ and $\frac{3}{7}$. As before, merging adjacent density distributions from different layers yields a phase with seven layers in which each layer has the same number of particles.

IV. DISCUSSION

The results of the simulations discussed in Sec. III admit the following generalization for the n-layer buckling transition: the longitudinal density distribution of each layer becomes bimodal with ratios of the particle populations given by

$$\left(\frac{n}{n+1}\right)\left(\frac{1}{n+1}\right),\left(\frac{n-1}{n+1}\right)\left(\frac{2}{n+1}\right),\ldots,\times\left(\frac{2}{n+1}\right)\left(\frac{n-1}{n+1}\right),\left(\frac{1}{n+1}\right)\left(\frac{n}{n+1}\right). \quad (4.1)$$

In Eq. (4.1), the ratio terms are ordered such that the leftmost term corresponds to the layer that is closest to one of the walls and the rightmost term to the layer that is closest to the other wall. There are n ratio terms in Eq. (4.1), corresponding to the n layers, and these terms are symmetric with respect to the midpoint of the set. This buckled phase mediates the structural conversion $n\triangle \rightarrow (n+1)\square$. The transition from an n-buckled phase to an $(n+1)\square$ phase occurs when adjacent peaks of the longitudinal density distributions of different layers combine to form $(n+1)$ layers with the same in-plane density. For a process at constant N and A, the in-plane density of a layer in the $(n+1)\square$ phase is smaller by factor of $n/(n+1)$ than what it was in the $n\triangle$ phase. The lateral structure of each layer displays l_{out} rows of particles that are displaced toward larger $|z^{*}|$ and $l_{\mathrm{in}}=n+1-l_{\mathrm{out}}$ rows of particles which are displaced toward smaller $|z^{*}|$, where l_{out} and l_{in} are the values of the numerators of the ratios given in Eq. (4.1).

Obviously the regularity of the structure of the sequence displayed in Eq. (4.1) cannot persist for n indefinitely large. As the number of layers increases the range of H in which the buckled phase is stable decreases, and that range eventually becomes equal to or less than the amplitude of out-of-plane thermal motion. Then the buckled phase becomes unstable with respect to a phase consisting of parallel planes of particles. This crossover resembles the situation that pertains for a one-layer system. In that case, when the spacing between the walls that confine it become smaller than some critical value, buckling of the one-layer system becomes unstable.

In the $1\triangle \rightarrow 2\square$ conversion through the one-layer buckled phase, a simple in-plane perpendicular reduction of the separation of the buckled rows is sufficient to convert the triangular packing of the particles to a square packing. For $2\triangle \rightarrow 3\square$ conversion via the two-layer buckled phase, the in-plane perpendicular reduction of the separation of the buckled rows converts half of the configuration to a triangular array and half to a square array, so another rearrangement between half of the rows must take place to complete the phase transition. For the conversion $3\triangle \rightarrow 4\square$, the same process leads to two-thirds of the configuration in a triangular array. Indeed, as the number of layers increases more rearrangements are required to complete the phase transition. It is possible that the character of this rearrangement is potential dependent, as we found for the $2\triangle \rightarrow 2\square$ transition, and that the phase transition can be either first order or continuous with intermediate states that are associated with the buckled phases.

ACKNOWLEDGMENTS

The research reported in this paper was supported by the National Science Foundation via Grant No. NSF CHE-9528923, with assistance from the Materials Research Science and Engineering Center at The University of Chicago, supported by Grant No. NSF DMR-9400379.

[1] J. Perrin, Ann. Chim. Phys. **18**, 1 (1909).
[2] B. Pansu, Pa. Pieranski, and L. Strzelecki, J. Phys. (Paris) **44**, 531 (1983).
[3] B. Pansu, Pi. Pieranski, and Pa. Pieranski, J. Phys. (Paris) **45**, 331 (1983).
[4] T. Ogawa, J. Phys. Soc. Jpn. Suppl. **52**, 167 (1983).
[5] D. H. van Winkle and C. A. Murray, Phys. Rev. A **34**, 562 (1986).
[6] C. Murray, W. Sprenger, R. Seshadri, and J. Cerise, in *Dynamics in Small Confining Systems*, edited by J. M. Drake, S. M. Trolan, J. Klafter, and R. Kopelman, MRS Symposia Proceedings No. 366 (Materials Research Society, Pittsburgh, 1995), p. 163.
[7] S. Neser, T. Palberg, and P. Leiderer, Prog. Colloid Polym. Sci. **104**, 194 (1997).
[8] T. Chou and D. R. Nelson, Phys. Rev. E **48**, 4611 (1993).
[9] M. Schmidt and H. Löwen, Phys. Rev. E **55**, 7228 (1997).
[10] R. R. Netz, in *The Structure and Conformation of Amphiphilic Membranes*, edited by R. Lipowsky, D. Richter, and K. Kremer, Springer Proceedings in Physics Vol. 66 (Springer-Verlag, Berlin, 1992).
[11] C. Cametti, F. D. Luca, A. D'Illario, G. Briganti, and M. A. Macri, in *The Structure and Conformation of Amphiphilic Membranes* (Ref. [10]).
[12] D. Rüppel and E. Sackmann, J. Phys. (Paris) **44**, 1025 (1983).
[13] A. Saint-Jalmes, F. Graner, and F. Gallet, Europhys. Lett. **28**, 565 (1994).
[14] R. Zangi and S. A. Rice, Phys. Rev. E **58**, 7529 (1998).